A nanowire optical nanocavity for broadband enhancement of spontaneous emission

Saptarshi Kotal, Alberto Artioli, Yujing Wang, Andreas Dyhl Osterkryger, Matteo Finazzer, Romain Fons, Yann Genuist, Joël Bleuse, Jean-Michel Gérard, Niels Gregersen, et al.

Applied Physics Letters ARTICLE scitation.org/journal/apl

A nanowire optical nanocavity for broadband enhancement of spontaneous emission

Cite as: Appl. Phys. Lett. **118**, 194002 (2021); doi: 10.1063/5.0045834
Submitted: 29 January 2021 · Accepted: 19 April 2021 ·
Published Online: 14 May 2021

View Online Export Citation CrossMark

Saptarshi Kotal,[1] Alberto Artioli,[1] Yujing Wang,[2] Andreas Dyhl Osterkryger,[2] Matteo Finazzer,[1] Romain Fons,[1] Yann Genuist,[3] Joël Bleuse,[1] Jean-Michel Gérard,[1] Niels Gregersen,[2] and Julien Claudon[1,a)]

AFFILIATIONS

[1]Univ. Grenoble Alpes, CEA, Grenoble INP, IRIG, PHELIQS, "Nanophysique et Semiconducteurs" Group, F-38000 Grenoble, France
[2]DTU Fotonik, Department of Photonics Engineering, Technical University of Denmark, DK-2800 Kongens Lyngby, Denmark
[3]Univ. Grenoble Alpes, CNRS, Grenoble INP, Institut Néel, "Nanophysique et Semiconducteurs" Group, F-38000 Grenoble, France

Note: This paper is part of the APL Special Collection on Non-Classical Light Emitters and Single-Photon Detectors.
[a)]**Author to whom correspondence should be addressed:** julien.claudon@cea.fr

ABSTRACT

To deliver an optimal performance for photonic quantum technologies, semiconductor quantum dots should be integrated in a carefully designed photonic structure. Here, we introduce a nanowire optical nanocavity designed for free-space emission. Thanks to its ultrasmall mode volume, this simple structure offers a large acceleration of spontaneous emission (predicted Purcell factor of 6.3) that is maintained over a 30-nm bandwidth. In addition, a dielectric screening effect strongly suppresses the emission into the 3D continuum of radiation modes. The fraction of spontaneous emission funneled into the cavity mode reaches 0.98 at resonance and exceeds 0.95 over a 100-nm spectral range. Close-to-optimal collection efficiency is maintained over an equivalent bandwidth and reaches a predicted value of 0.54 at resonance for a first lens with a numerical aperture (NA) of 0.75. As a first experimental demonstration of this concept, we fabricate an Au–SiO_2–GaAs device embedding isolated InAs quantum dots. We measure a maximal acceleration of spontaneous emission by a factor as large as 5.6 and a bright quantum dot emission (collection efficiency of 0.35 into NA = 0.75). This nanowire cavity constitutes a promising building block to realize advanced sources of quantum light for a broad range of material systems.

Semiconductor quantum dots (QDs) have enabled major contributions to photonic quantum technologies.[1] These solid-state artificial atoms can emit various non-classical states of light on-demand and with high fidelity,[2–4] or implement optical nonlinearities at a few-photon level.[5–8] State-of-the-art devices generally employ a photonic nanostructure that defines a controlled electromagnetic environment around the QD.[8–29] First of all, such a control aims at optimizing light collection in the channel of interest. Some structures additionally leverage a local increase in the density of optical states to accelerate the QD spontaneous emission (SE), thereby mitigating the detrimental impact of noise sources that are inherent to a solid-state environment. Ideally, SE acceleration and large collection efficiency should be maintained over a broad operation bandwidth. Such a combination is key to realize widely tunable sources of indistinguishable single photons or bright sources of pairs of entangled and indistinguishable photons.[28,29] In practice, however, existing approaches often compromise between these three desirable features. Microcavities exploit the Purcell effect to provide large SE acceleration and efficient light collection, but only on a narrow spectral range defined by the cavity linewidth.[9–16] In contrast, waveguides offer a broadband collection efficiency with generally limited SE enhancement.[8,17–25] Nanocavities potentially combine the assets of these two mainstream approaches. Thanks to their ultrasmall mode volume, nanocavities indeed provide a large Purcell acceleration with a moderate optical quality factor, which directly translates into a large operation bandwidth. This strategy inspired several proposals,[30–33] but only a few broadband QD nanocavity devices have been demonstrated so far, using photonic crystals[26] or bullseye structures.[27–29]

In this Letter, we introduce a nanowire optical nanocavity that is designed for free-space emission [Fig. 1(a)]. Despite its simplicity, this structure offers a large SE enhancement (predicted Purcell factor $F_p = 6.3$) that is maintained over a bandwidth of 30 nm. This approach also benefits from a pronounced dielectric screening effect, which largely suppresses SE into the 3D continuum of radiation modes. As a result, the fraction β of SE funneled into the cavity mode reaches 0.98 at resonance and exceeds 0.95 over a 100-nm spectral

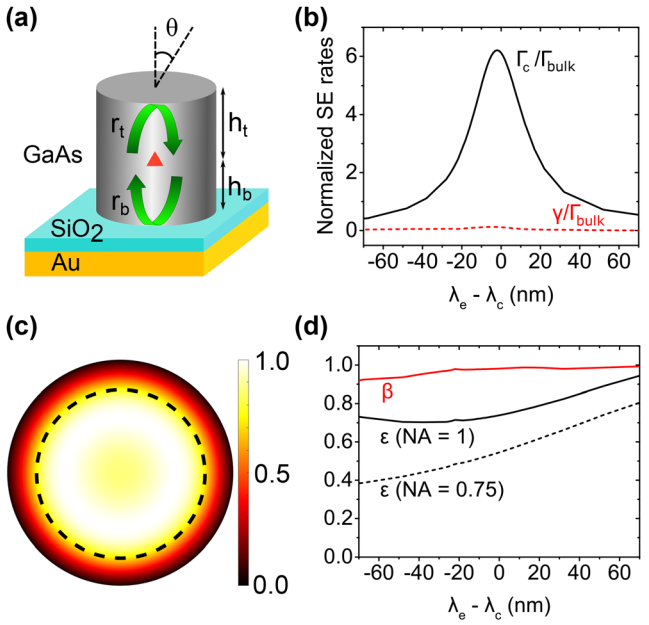

FIG. 1. (a) Schematics of the nanowire nanocavity. (b) Normalized SE rates into the cavity mode (Γ_c/Γ_{bulk}) and into the 3D continuum of radiation modes (γ/Γ_{bulk}) calculated as a function of the emitter-cavity wavelength detuning ($\lambda_e - \lambda_c$). (c) Map of the angular distribution of the far-field emission for a QD at resonance ($\lambda_e = \lambda_c$). The dashed circle corresponds to a numerical aperture NA = sin (θ_{max}) = 0.75 and the external one to NA = 1. (d) Fraction β of SE funneled into the cavity mode and first lens collection efficiency ϵ (for NA = 0.75 and 1), as a function of ($\lambda_e - \lambda_c$). All calculations are conducted for an on-axis emitter; geometrical parameters: $h_b = 70$ nm, $h_t = 390$ nm, and $d = 245$ nm, which leads to a cavity resonance at $\lambda_c = 928$ nm.

range. Optimal collection efficiency is maintained over a similar bandwidth, with a calculated value of 0.54 at resonance for a first lens with a numerical aperture (NA) = 0.75. As a first demonstration of this concept, we fabricate an Au–SiO_2–GaAs device embedding isolated InAs QDs. We measure an SE acceleration factor as large as 5.6 and obtain bright QD emission (collection efficiency up to 0.35 for a first lens having NA = 0.75).

As schematized in Fig. 1(a), the proposed device consists of a segment of a cylindrical nanowire of diameter d, which is made of a material having a large refractive index n (here GaAs, $n = 3.46$). The nanowire stands on a SiO_2–Au planar mirror[34] and is terminated by a flat top facet: these two elements provide broadband reflectivity. The cavity mode of interest can be roughly described by considering the Fabry–Pérot reflections of HE_{11}, the fundamental mode guided by the GaAs section. We consider below a nanocavity mode with three longitudinal antinodes and note λ_c its resonance wavelength. The nanocavity embeds a QD (emission wavelength λ_e) that is modeled as a point-like optical emitter with two transverse and mutually orthogonal linear dipole components. In the following, the QD SE rate in bulk GaAs, Γ_{bulk}, serves as a reference. For a resonant QD ($\lambda_e = \lambda_c$) that sits on one of the antinodes, the normalized SE rate into the cavity mode Γ_c/Γ_{bulk} reaches a maximum value that is equal to F_p, the nanocavity Purcell factor.

We first estimate F_p with a simple single-mode model[32,35]

$$F_p = \frac{\Gamma_{HE_{11}}}{\Gamma_{bulk}} \times \frac{(1+|r_b|)(1+|r_t|)}{1-|r_b r_t|}. \quad (1)$$

Here, $\Gamma_{HE_{11}}$ is the SE rate of an on-axis emitter into the fundamental mode guided by an infinitely long nanowire. r_b (r_t) is the modal amplitude reflectivity of the HE_{11} mode for the bottom (top) extremity. In the supplementary material, we plot ($\Gamma_{HE_{11}}/\Gamma_{bulk}$), $|r_b|^2$, and $|r_t|^2$ as a function of the reduced diameter d/λ. We choose here $d = 0.26\lambda_e$, which simultaneously ensures a significant top facet reflectivity ($|r_t|^2 = 0.43$) and good coupling to HE_{11} ($\Gamma_{HE_{11}}/\Gamma_{bulk} = 0.86$). In this diameter range, the bottom reflectivity ($|r_b|^2 = 0.9$) is optimized for a 7-nm-thick silica spacer. This yields a nanocavity Purcell factor as large as $F_p = 7.3$. At the same time, the $|r_t|^2$ is small enough to (i) ensure a modest optical quality factor ($Q \sim 30$) or, equivalently, a large operation bandwidth and (ii) keep losses in the bottom mirror at a reasonable level and preserve the collection efficiency.

In reality, the single-mode model does not accurately describe the nanocavity mode, due to the (small) coupling of HE_{11} to weakly guided or non-guided modes upon reflection on the facets. This interesting property will be extensively addressed in a future paper. For now, we present results obtained with a Fourier modal method implementing open geometry boundary conditions,[36,37] which permits to take into account the coupling of the emitter to all modes, including radiation modes. The QD is here located at the first longitudinal antinode of the nanocavity mode, at a distance $h_b = 70$ nm ($h_t = 390$ nm) from the bottom (top) mirror. These dimensions correspond to the fabricated devices discussed in the second part of this Letter. For $d = 245$ nm, the cavity resonance is found at $\lambda_c = 928$ nm. Figure 1(b) shows Γ_c/Γ_{bulk} as a function of ($\lambda_e - \lambda_c$). On resonance, $\Gamma_c/\Gamma_{bulk} = 6.3$. This value—slightly below the single-mode prediction—remains remarkably high for such a simple structure. Furthermore, a pronounced SE acceleration is maintained over a 30 nm-large bandwidth [full width at half maximum (FWHM)]. Figure 1(b) also shows γ/Γ_{bulk}, the normalized emission rate into the 3D continuum of radiation modes. Thanks to a strong dielectric screening effect,[38–40] $\gamma/\Gamma_{bulk} \ll 1$ over an even larger spectral range. As a result, the fraction $\beta = \Gamma_c/(\Gamma_c + \gamma)$ of SE funneled into the cavity mode is as high as 0.98 at resonance and exceeds 0.95 over a 100-nm spectral range [Fig. 1(d)].

As evidenced in Fig. 1(d), a broadband β factor directly translates into a broadband collection efficiency ϵ. At resonance, one obtains ϵ as large as 0.54, using a first lens with NA = 0.75. To shed light on loss channels, we also plot a calculation of ϵ for NA = 1. First, the difference 1- ϵ(NA = 1) corresponds to absorption losses upon reflection on the bottom gold layer. Second, a comparison of ϵ for the two NA's shows that the output beam is directional: more than 70% of the photons emitted upward can be collected with NA = 0.75. This is confirmed by Fig. 1(c), which shows the angular profile of the device output beam for a QD at resonance. We note that this profile results from the subtle interplay between several contributions (scattering and reflection by the top facet) and involves interference associated with the reflection on the bottom mirror. A detailed optimization (left for a future work) could further increase the beam directionality and in turn the collection efficiency for moderate collection NA.

Starting from a planar structure grown by molecular beam epitaxy, we used a top-down process to fabricate arrays of GaAs nanocavities embedding self-assembled InAs QDs (see the supplementary

material). A nanocavity of diameter close to 240 nm resonates around 920 nm, which corresponds to the peak of the QD ensemble emission. A device, such as the one shown in Fig. 2(a), typically contains ∼5 QDs. Their emission wavelengths as well as their lateral positions in the nanocavity section are randomly distributed. Nevertheless, thanks to the broad operation bandwidth of the nanocavity, a large fraction of the QDs experience a significant coupling to the cavity mode. As detailed in the supplementary material, we estimate that 1 QD out of 10 features $\Gamma_c > \frac{1}{2}\max(\Gamma_c)$. In terms of collection efficiency, the tolerance is even larger, thanks to the pronounced inhibition of SE into "unwanted" modes.

The nanocavity chip is mounted on the cold finger of a helium flow cryostat ($T = 4$ K) featuring an optical access. Non-resonant excitation is provided by a pulsed Ti:sapphire laser (excitation wavelength, 820 nm; FWHM pulse duration, 200 fs; repetition rate, 76 MHz). The excitation beam is focused on the structure with a microscope objective (NA = 0.75), which also collects the luminescence signal of the device. Photoluminescence spectra are acquired with a grating spectrometer (1200 grooves/mm; 64-cm focal length) equipped with a silicon charge-coupled device camera. A rotating $\lambda/2$ waveplate and a fixed linear polarizer placed before the spectrometer can be used to analyze the polarization of the device emission. Time-resolved measurements are performed with a fast silicon avalanche photodiode. A measurement of the instrument response function with attenuated laser pulses (tuned to 920 nm) is shown in Fig. 3. It yields a temporal resolution of 80 ps (FWHM) and reveals a long-delay tail attributed to carrier detraping in the active layer of the avalanche photodiode. The complete instrument response function is systematically convoluted with the exponential decay functions used to fit time-resolved experimental data.

We first focus on a nanocavity device that directly illustrates the broad operation bandwidth. The corresponding photoluminescence spectrum is shown in Fig. 2(b). It features narrow emission lines, attributed to the recombination of excitonic complexes trapped in several QDs. In the following, we focus on the bright lines labeled QD1 and QD2, whose emission wavelengths differ by 13 nm. Figure 2(c) shows their spectrally integrated intensity I as a function of the excitation power P_{exc}. I is obtained by fitting each emission line to a Lorentzian spectral profile and by summing the contributions of two spectra acquired for two angles of the $\lambda/2$ waveplate that differ by 45°. This procedure allows taking into account a weak polarization of the nanocavity emission. For low excitation powers, I exhibits a linear power dependence for both lines. Next, the emission spectrum for various polarization analysis angles is closely inspected to check the presence of a fine structure splitting. QD1 shows such a splitting and is attributed to a neutral exciton, while QD2 is associated with a charged exciton. Over the complete range of excitation powers, the measured integrated intensities are perfectly reproduced by $I(P_{exc}) = I_{sat}[1 - \exp(-P_{exc}/P_{sat})]$, with P_{sat} the saturation power and I_{sat} the integrated intensity at saturation. Despite vastly different emission wavelengths, QD1 and QD2 feature similar I_{sat}: this is a signature of broadband collection efficiency.

We next quantify the Purcell acceleration provided by the nanocavity. Because of the very large cavity mode linewidth, it is not possible to tune the same emitter on and off resonance using, e.g., temperature. Instead, we compare the radiative rate of nanocavity QDs to the one of similar QDs embedded in bulk GaAs. This reference rate Γ_{bulk} is determined as follows. We measure the photoluminescence decay of an ensemble of QDs embedded in the middle of large ($20 \times 20\ \mu m^2$) squares that are also patterned on the nanocavity chip. A representative measurement shown in Fig. 3 reveals a bi-exponential decay, which is typical of interconversions between the bright and dark excitons hosted by neutral QDs. A fit of the data to $A_+ \exp(-\Gamma_+ t) + A_- \exp(-\Gamma_- t)$ yields the two decay rates Γ_+ and Γ_- ($\Gamma_+ > \Gamma_-$). The radiative rate is then determined with a simple three-level model. The two bright excitonic states are treated as a single level, which decays radiatively to the QD ground state with a rate Γ_r.

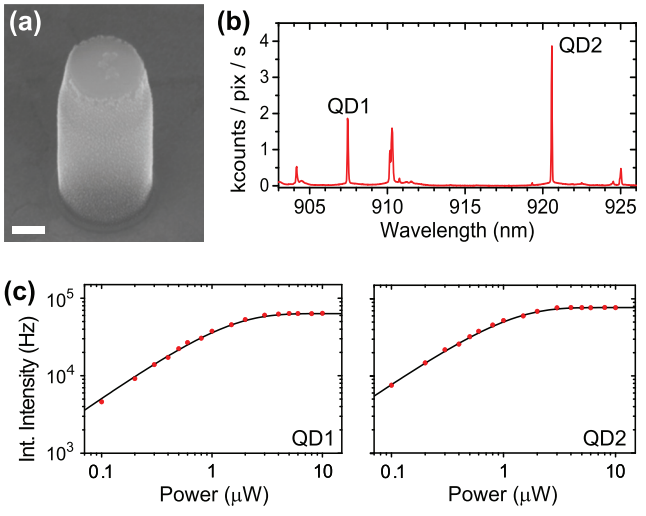

FIG. 2. (a) Scanning electron microscope image of a representative device (tilted view; scale bar, 100 nm). (b) Micro-photoluminescence spectrum as measured on the CCD under pulsed excitation ($P_{exc} = 300$ nW) at $T = 4$ K. (c) Spectrally integrated intensity I of lines QD1 and QD2 as a function of P_{exc}. The dots correspond to experiments and the solid line to theory (see the text for details).

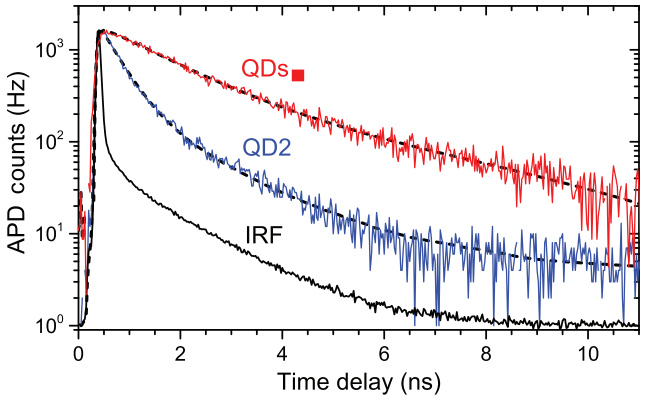

FIG. 3. Time-resolved measurements. "IRF": measured instrument response function. "QD2": individual emission line identified in Fig. 2(b) (solid blue line: experimental data; dashed line: fit to a single-exponential decay convoluted with the IRF). "QDs■": ensemble of QDs embedded in a large square ($20 \times 20\ \mu m^2$) (solid red line: experimental data; dashed line: fit to a bi-exponential decay convoluted with the IRF). This measurement is used to determine the reference rate Γ_{bulk} (see the text for details).

Similarly, the two dark excitonic states are treated as a single level. The bright-to-dark and dark-to-bright spinflip processes are characterized by the same rate $\gamma_{\downarrow}$, and we neglect other non-radiative processes. Within these hypotheses, the two rates Γ_+ and Γ_- are given by $\Gamma_{\pm} = \frac{1}{2}[\Gamma_r + 2\gamma_{\downarrow} \pm (\Gamma_r^2 + 4\gamma_{\downarrow}^2)^{1/2}]$. After determining Γ_r, we compensate for the small SE acceleration provided by the planar structure, by a calculated factor of 1.32. We repeat ~20 measurements and obtain with this procedure the average value $\Gamma_{\text{bulk}} = 0.61\,\text{ns}^{-1}$ (standard deviation of $0.05\,\text{ns}^{-1}$).

In the nanocavity, QD1 and QD2 exhibit much faster radiative dynamics. Figure 3 shows time-resolved data associated with QD2. As expected for a charged exciton, it features a single-exponential decay. A fit of the data to $A\exp(-\Gamma_r t)$ directly yields the radiative decay rate $\Gamma_r = 3.0\,\text{ns}^{-1}$, a value that exceeds Γ_{bulk} by a factor of 5 (charged and neutral excitons feature similar oscillator strength[41]). The decay curve of QD1 is bi-exponential (not shown). As mentioned above, this feature is characteristic of the interconversion between the bright and dark excitons states hosted by a neutral QD. We use again a fit to a bi-exponential decay function and the simple three-level model to determine $\Gamma_r = 2.4\,\text{ns}^{-1}$, which amounts to $4 \times \Gamma_{\text{bulk}}$. Despite vastly different emission wavelengths, QD1 and QD2 display a pronounced SE acceleration: this directly evidences the broadband Purcell effect provided by the nanocavity. Figure 4(a) summarizes results obtained on 10 excitonic lines (three charged and seven neutral excitons) measured in six similar devices. Large SE accelerations are routinely observed. The fastest measured line features $\Gamma_r/\Gamma_{\text{bulk}} = 5.6$, thus approaching the predicted maximum radiative rate.

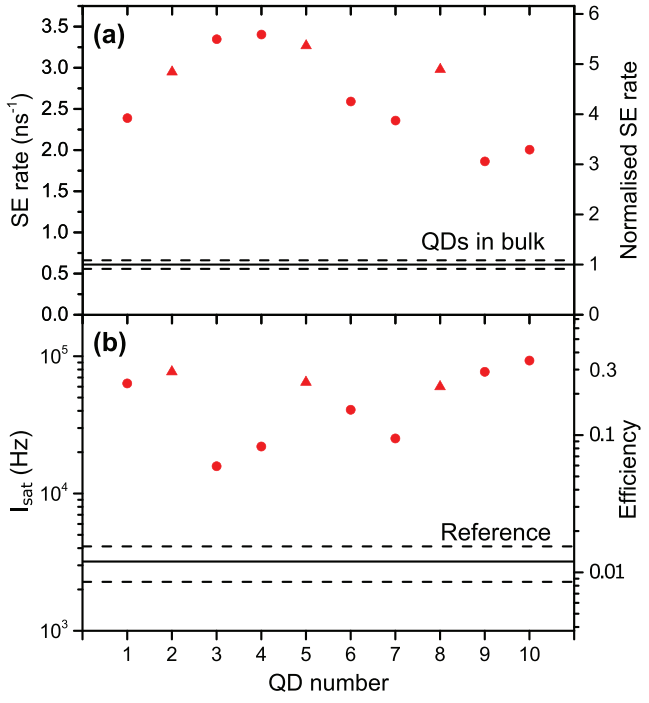

FIG. 4. Acceleration of spontaneous emission (a) and collection efficiency (b) for the 10 selected QD emission lines, belonging to six distinct nanocavities. Disks (triangles) correspond to neutral (charged) excitons. QD1 and QD2 correspond to the emission lines identified in Fig. 2(b). In panel (a), the spontaneous emission rate of similar QDs embedded in bulk GaAs serves as a reference (horizontal solid line: mean value; dashed lines: ±1 std). In panel (b), the reference for the intensity at saturation (I_{sat}) is measured on individual dots embedded in a low-density sample (horizontal solid line: mean value; dashed lines: ±1 std). See main text for details.

To determine the source brightness, we compare the saturation intensities I_{sat} of QD1 and QD2 to the one of a QD embedded in an unprocessed environment. Our reference is an isolated InAs QD embedded in a planar GaAs layer and located 120 nm below the air–semiconductor interface. It features a calculated collection efficiency $\epsilon_{\text{ref}} = 1.2 \times 10^{-2}$ for a first lens with NA = 0.75. In practice, the reference sample was grown by molecular beam epitaxy and belongs to a "border zone," where the QD areal density is low enough to ensure that single emitters can be isolated under the microscope excitation spot. We note that such QDs generally feature a significantly polarized emission, as observed earlier.[42] By studying several isolated QDs, we determine a mean reference value at saturation $I_{\text{sat,ref}} = 3.2\,\text{kHz}$ (standard deviation of 0.9 kHz). For QD1 (QD2), we measure $I_{\text{sat}} = 64\,\text{kHz}$ ($I_{\text{sat}} = 77\,\text{kHz}$). This corresponds to a brightness improvement by a factor of 20 (24) and yields a collection efficiency of 0.24 (0.29) for a first lens with NA = 0.75. Figure 4(b) summarizes brightness measurements conducted on several nanocavities. The brightest line features a collection efficiency as high as 0.35.

This figure of merit could be further improved to reach the theoretical limit by stabilizing the QD charge state[41] and/or by employing deterministic fabrication techniques. The top-down fabrication route used in this work could be refined by performing cathodo- or photoluminescence imaging, followed by an aligned e-beam lithography to define a nanocavity around selected self-assembled QDs.[27,43] A bottom-up approach represents an appealing alternative for deterministic fabrication. A two-step core–shell growth has already been employed to realize nanowire antennas embedding a single, on-axis QD.[19,21,23] Furthermore, the nanowire nucleation site can be controlled through a proper patterning of the growth substrate.[21,44,45]

To conclude, we have introduced and demonstrated a nanocavity which provides large SE acceleration and collection efficiency over a broad spectral range. These are key assets to realize a bright and widely tunable source of indistinguishable single photons, for example by applying mechanical stress on the QD with an integrated piezoactuator.[46] We note that thanks to its nanoscale volume, the proposed nanocavity additionally features a small sensitivity to the QD spectral broadening associated with low-frequency thermal vibrations.[47] In the future, elliptical nanocavities could provide a full control over the polarization of the emitted photons, in analogy with previous work on nanowire antennas.[20] The proposed nanocavity is also promising for the emission of pairs of polarization-entangled and indistinguishable photons. Beyond advanced quantum light sources, this broadband photonic structure could enhance optical non-linearities involving several detuned QD transitions[7] or be used to explore subtle nonresonant couplings between distinct QDs.[48] Finally, from a technological point of view, the relative simplicity of the device makes it also very appealing for emergent material systems, which are not yet as technologically mature as III-As semiconductors.

See the supplementary material for (i) the calculated diameter dependence of $(\Gamma_{\text{HE}_{11}}/\Gamma_{\text{bulk}})$, $|r_b|^2$, and $|r_t|^2$, (ii) the calculated β factor and collection efficiency for off-axis emitters, (iii) the fabrication process, and (iv) an estimation of the device fabrication yield.

This work was supported by the French Agence Nationale de la Recherche (ANR) (Grant No. ANR-19-CE47-0009-02), the Independent Research Fund Denmark (Grant No. DFF 4005-00370), and the European Union's Horizon 2020 (No. EU-H2020) research and innovation program under the Marie Skłodowska-Curie (MSC) Grant Agreement No. 861097. S.K. acknowledges support from the EU-H2020 research and innovation program under MSC Grant Agreement No. 754303 and the French ANR under the program "Investissements d'avenir" (No. ANR-15-IDEX-02). The authors thank Eric Delamadeleine, Tomasz Jakubczyk, and Marlène Terrier for the contribution to sample processing. Sample fabrication was carried out in the "Plateforme Technologique Amont" clean room.

DATA AVAILABILITY

The data that support the findings of this study are available from the corresponding author upon reasonable request.

REFERENCES

[1]P. Lodahl, S. Mahmoodian, and S. Stobbe, "Interfacing single photons and single quantum dots with photonic nanostructures," Rev. Mod. Phys. **87**, 347–400 (2015).
[2]P. Senellart, G. Solomon, and A. White, "High-performance semiconductor quantum-dot single-photon sources," Nat. Nanotechnol. **12**, 1026–1039 (2017).
[3]D. Huber, M. Reindl, J. Aberl, A. Rastelli, and R. Trotta, "Semiconductor quantum dots as an ideal source of polarization-entangled photon pairs on-demand: A review," J. Opt. **20**, 073002 (2018).
[4]I. Schwartz, D. Cogan, E. R. Schmidgall, Y. Don, L. Gantz, O. Kenneth, N. H. Lindner, and D. Gershoni, "Deterministic generation of a cluster state of entangled photons," Science **354**, 434–437 (2016).
[5]D. Englund, A. Faraon, I. Fushman, N. Stoltz, P. Petroff, and J. Vučković, "Controlling cavity reflectivity with a single quantum dot," Nature **450**, 857 (2007).
[6]A. Javadi, I. Söllner, M. Arcari, S. Lindskov Hansen, L. Midolo, S. Mahmoodian, G. Kirsanske, T. Pregnolato, E. H. Lee, J. D. Song, S. Stobbe, and P. Lodahl, "Single-photon non-linear optics with a quantum dot in a waveguide," Nat. Commun. **6**, 8655 (2015).
[7]H. A. Nguyen, T. Grange, B. Reznychenko, I. Yeo, P.-L. de Assis, D. Tumanov, F. Fratini, N. S. Malik, E. Dupuy, N. Gregersen, A. Auffèves, J.-M. Gérard, J. Claudon, and J.-P. Poizat, "Giant non-linear interaction between two optical beams via a quantum dot embedded in a photonic wire," Phys. Rev. B **97**, 201106(R) (2018).
[8]H. Thyrrestrup, G. Kiršanskė, H. L. Jeannic, T. Pregnolato, L. Zhai, L. Raahauge, L. Midolo, N. Rotenberg, A. Javadi, R. Schott, A. D. Wieck, A. Ludwig, M. C. Löbl, I. Söllner, R. J. Warburton, and P. Lodahl, "Quantum optics with near-lifetime-limited quantum-dot transitions in a nanophotonic waveguide," Nano Lett. **18**, 1801–1806 (2018).
[9]J. M. Gérard, B. Sermage, B. Gayral, B. Legrand, E. Costard, and V. Thierry-Mieg, "Enhanced spontaneous emission by quantum boxes in a monolithic optical microcavity," Phys. Rev. Lett. **81**, 1110 (1998).
[10]P. Michler, A. Kiraz, C. Becher, W. V. Schoenfeld, P. M. Petroff, L. Zhang, E. Hu, and A. Imamoğlu, "A quantum dot single-photon turnstile device," Science **290**, 2282 (2000).
[11]C. Santori, D. Fattal, J. Vučković, G. S. Solomon, and Y. Yamamoto, "Indistinguishable photons from a single-photon device," Nature **419**, 594 (2002).
[12]M. Pelton, C. Santori, J. Vučković, B. Zhang, G. S. Solomon, J. Plant, and Y. Yamamoto, "Efficient source of single photons: A single quantum dot in a micropost microcavity," Phys. Rev. Lett. **89**, 233602 (2002).
[13]J.-M. Gérard, "Solid-state cavity-quantum electrodynamics with self-assembled quantum dots," in *Single Quantum Dots: Fundamentals, Applications, and New Concepts* (Springer, Berlin Heidelberg, 2009); Top. Appl. Phys. **90**, 269–314 (2003).
[14]S. Strauf, N. G. Stoltz, M. T. Rakher, L. A. Coldren, P. M. Petroff, and D. Bouwmeester, "High-frequency single–photon source with polarization control," Nat. Photonics **1**, 704 (2007).
[15]N. Somaschi, V. Giesz, L. De Santis, J. C. Loredo, M. P. Almeida, G. Hornecker, S. L. Portalupi, T. Grange, C. Antón, J. Demory, C. Gómez, I. Sagnes, N. D. Lanzillotti-Kimura, A. Lemaître, A. Auffèves, A. G. White, L. Lanco, and P. Senellart, "Near-optimal single-photon sources in the solid state," Nat. Photonics **10**, 340–345 (2016).
[16]X. Ding, Y. He, Z.-C. Duan, N. Gregersen, M.-C. Chen, S. Unsleber, S. Maier, C. Schneider, M. Kamp, S. Höfling, C.-Y. Lu, and J.-W. Pan, "On-demand single photons with high extraction efficiency and near-unity indistinguishability from a resonantly driven quantum dot in a micropillar," Phys. Rev. Lett. **116**, 020401 (2016).
[17]T. Lund-Hansen, S. Stobbe, B. Julsgaard, H. Thyrrestrup, T. Sünner, M. Kamp, A. Forchel, and P. Lodahl, "Experimental realization of highly efficient broadband coupling of single quantum dots to a photonic crystal waveguide," Phys. Rev. Lett. **101**, 113903 (2008).
[18]J. Claudon, J. Bleuse, N. S. Malik, M. Bazin, P. Jaffrennou, N. Gregersen, C. Sauvan, P. Lalanne, and J.-M. Gérard, "A highly efficient single-photon source based on a quantum dot in a photonic nanowire," Nat. Photonics **4**, 174–177 (2010).
[19]M. E. Reimer, G. Bulgarini, N. Akopian, M. Hocevar, M. B. Bavinck, M. A. Verheijen, E. P. A. M. Bakkers, L. P. Kouwenhoven, and V. Zwiller, "Bright single-photon sources in bottom-up tailored nanowires," Nat. Commun. **3**, 737 (2012).
[20]M. Munsch, J. Claudon, J. Bleuse, N. S. Malik, E. Dupuy, J.-M. Gérard, Y. Chen, N. Gregersen, and J. Mørk, "Linearly polarized, single-mode spontaneous emission in a photonic nanowire," Phys. Rev. Lett. **108**, 077405 (2012).
[21]D. Dalacu, K. Mnaymneh, J. Lapointe, X. Wu, P. J. Poole, G. Bulgarini, V. Zwiller, and M. E. Reimer, "Ultraclean emission from InAsP quantum dots in defect-free wurtzite InP nanowires," Nano Lett. **12**, 5919 (2012).
[22]M. N. Makhonin, J. E. Dixon, R. J. Coles, B. Royall, E. Clarke, M. S. Skolnick, and A. M. Fox, "On-chip resonantly-driven quantum emitter with enhanced coherence," Nano Lett. **14**, 6997 (2014).
[23]M. A. M. Versteegh, M. E. Reimer, K. D. Jöns, D. Dalacu, P. J. Poole, A. Gulinatti, A. Giudice, and V. Zwiller, "Observation of strongly entangled photon pairs from a nanowire quantum dot," Nat. Commun. **5**, 5298 (2014).
[24]P. Stepanov, A. Delga, X. Zang, J. Bleuse, E. Dupuy, E. Peinke, P. Lalanne, J.-M. Gérard, and J. Claudon, "Quantum dot spontaneous emission control in a ridge waveguide," Appl. Phys. Lett. **106**, 041112 (2015).
[25]A. W. Elshaari, E. Büyüközer, I. Esmaeil Zadeh, T. Lettner, P. Zhao, E. Schöll, S. Gyger, M. E. Reimer, D. Dalacu, P. J. Poole, K. D. Jöns, and V. Zwiller, "Strain-tunable quantum integrated photonics," Nano Lett. **18**, 7969–7976 (2018).
[26]F. Liu, A. J. Brash, J. O'Hara, L. M. P. P. Martins, C. L. Phillips, R. J. Coles, B. Royall, E. Clarke, C. Bentham, N. Prtljaga, I. E. Itskevich, L. R. Wilson, M. S. Skolnick, and A. M. Fox, "High Purcell factor generation of indistinguishable on-chip single photons," Nat. Nanotechnol. **13**, 835–840 (2018).
[27]L. Sapienza, M. Davanco, A. Badolato, and K. Srinivasan, "Nanoscale optical positioning of single quantum dots for bright and pure single-photon emission," Nat. Commun. **6**, 7833 (2015).
[28]J. Liu, R. Su, Y. Wei, B. Yao, S. F. Covre da Silva, Y. Yu, J. Iles-Smith, K. Srinivasan, A. Rastelli, J. Li, and X. Wang, "A solid-state source of strongly entangled photon pairs with high brightness and indistinguishability," Nat. Nanotechnol. **14**, 586–593 (2019).
[29]H. Wang, H. Hu, T.-H. Chung, J. Qin, X. Yang, J.-P. Li, R.-Z. Liu, H.-S. Zhong, Y.-M. He, X. Ding, Y.-H. Deng, Q. Dai, Y.-H. Huo, S. Höfling, C.-Y. Lu, and J.-W. Pan, "On-demand semiconductor source of entangled photons which simultaneously has high fidelity, efficiency, and indistinguishability," Phys. Rev. Lett. **122**, 113602 (2019).
[30]I. S. Maksymov, M. Besbes, J. P. Hugonin, J. Yang, A. Beveratos, I. Sagnes, I. Robert-Philip, and P. Lalanne, "Metal-coated nanocylinder cavity for broadband nonclassical light emission," Phys. Rev. Lett. **105**, 180502 (2010).
[31]X.-W. Chen, M. Agio, and V. Sandoghdar, "Metallodielectric hybrid antennas for ultrastrong enhancement of spontaneous emission," Phys. Rev. Lett. **108**, 233001 (2012).

[32]N. Gregersen, D. P. S. McCutcheon, J. Mørk, J.-M. Gérard, and J. Claudon, "A broadband tapered nanocavity for efficient nonclassical light emission," Opt. Express **24**, 20904 (2016).
[33]A. D. Osterkryger, J. Claudon, J.-M. Gérard, and N. Gregersen, "Photonic 'hourglass' design for efficient quantum light emission," Opt. Lett. **44**, 2617–2620 (2019).
[34]I. Friedler, P. Lalanne, J. P. Hugonin, J. Claudon, J. M. Gérard, A. Beveratos, and I. Robert-Philip, "Efficient photonic mirrors for semiconductor nanowires," Opt. Lett. **33**, 2635 (2008).
[35]I. Friedler, C. Sauvan, J. P. Hugonin, P. Lalanne, J. Claudon, and J. M. Gérard, "Solid-state single photon sources: The nanowire antenna," Opt. Express **17**, 2095 (2009).
[36]T. Häyrynen, J. R. de Lasson, and N. Gregersen, "Open-geometry Fourier modal method: Modeling nanophotonic structures in infinite domains," J. Opt. Soc. Am. A **33**, 1298–1306 (2016).
[37]U. M. Gür, S. Arslanagić, M. Mattes, and N. Gregersen, "Open-geometry modal method based on transverse electric and transverse magnetic mode expansion for orthogonal curvilinear coordinates," Phys. Rev. E **103**, 033301 (2021).
[38]J. Bleuse, J. Claudon, M. Creasey, N. S. Malik, J.-M. Gérard, I. Maksymov, J.-P. Hugonin, and P. Lalanne, "Inhibition, enhancement, and control of spontaneous emission in photonic nanowires," Phys. Rev. Lett. **106**, 103601 (2011).
[39]G. Bulgarini, M. E. Reimer, T. Zehender, M. Hocevar, E. P. A. M. Bakkers, L. P. Kouwenhoven, and V. Zwiller, "Spontaneous emission control of single quantum dots in bottom-up nanowire waveguides," Appl. Phys. Lett. **100**, 121106 (2012).
[40]J. Claudon, N. Gregersen, P. Lalanne, and J.-M. Gérard, "Harnessing light with photonic nanowires: Fundamentals and applications to quantum optics," ChemPhysChem **14**, 2393–2402 (2013).
[41]P. A. Dalgarno, J. M. Smith, J. McFarlane, B. D. Gerardot, K. Karrai, A. Badolato, P. M. Petroff, and R. J. Warburton, "Coulomb interactions in single charged self-assembled quantum dots: Radiative lifetime and recombination energy," Phys. Rev. B **77**, 245311 (2008).
[42]I. Favero, G. Cassabois, A. Jankovic, R. Ferreira, D. Darson, C. Voisin, C. Delalande, P. Roussignol, A. Badolato, P. M. Petroff, and J. M. Gérard, "Giant optical anisotropy in a single InAs quantum dot in a very dilute quantum-dot ensemble," Appl. Phys. Lett. **86**, 041904 (2005).
[43]M. Gschrey, A. Thoma, P. Schnauber, M. Seifried, R. Schmidt, B. Wohlfeil, L. Krüger, J. H. Schulze, T. Heindel, S. Burger, F. Schmidt, A. Strittmatter, S. Rodt, and S. Reitzenstein, "Highly indistinguishable photons from deterministic quantum-dot microlenses utilizing three-dimensional in situ electron-beam lithography," Nat. Commun. **6**, 7662 (2015).
[44]S. N. Dorenbos, H. Sasakura, M. P. van Kouwen, N. Akopian, S. Adachi, N. Namekata, M. Jo, J. Motohisa, Y. Kobayashi, K. Tomioka, T. Fukui, S. Inoue, H. Kumano, C. M. Natarajan, R. H. Hadfield, T. Zijlstra, T. M. Klapwijk, V. Zwiller, and I. Suemune, "Position controlled nanowires for infrared single photon emission," Appl. Phys. Lett. **97**, 171106 (2010).
[45]Z. Gacević, M. Holmes, E. Chernysheva, M. Müller, A. Torres-Pardo, P. Veit, F. Bertram, J. Christen, J. M. González Calbet, Y. Arakawa, E. Calleja, and S. Lazić, "Emission of linearly polarized single photons from quantum dots contained in nonpolar, semipolar, and polar sections of pencil-like InGaN/GaN nanowires," ACS Photonics **4**, 657–664 (2017).
[46]J. Martín-Sánchez, R. Trotta, A. Mariscal, R. Serna, G. Piredda, S. Stroj, J. Edlinger, C. Schimpf, J. Aberl, T. Lettner, J. Wildmann, H. Huang, X. Yuan, D. Ziss, J. Stangl, and A. Rastelli, "Strain-tuning of the optical properties of semiconductor nanomaterials by integration onto piezoelectric actuators," Semicond. Sci. Technol. **33**, 013001 (2018).
[47]A. Artioli, S. Kotal, N. Gregersen, P. Verlot, J.-M. Gérard, and J. Claudon, "Design of quantum dot-nanowire single-photon sources that are immune to thermomechanical decoherence," Phys. Rev. Lett. **123**, 247403 (2019).
[48]Q. Mermillod, T. Jakubczyk, V. Delmonte, A. Delga, E. Peinke, J.-M. Gérard, J. Claudon, and J. Kasprzak, "Harvesting, coupling, and control of single-exciton coherences in photonic waveguide antennas," Phys. Rev. Lett. **116**, 163903 (2016).